Journal of Superconductivity: Incorporating Novel Magnetism, Vol. 13, No. 2, 2000

Electrical and Thermal Transport in Perovskite Manganites

J. L. Cohn[1]

Experimental data on the temperature, magnetic field, and pressure dependencies of charge and heat transport in perovskite manganites, $A_{1-x}A'_xMnO_3$, are reviewed. The transport mechanisms in the paramagnetic, ferromagnetic and charge-ordered states are discussed and the role of double-exchange interactions and lattice-distortions emphasized.

KEY WORDS: Electrical and thermal transport; perovskite manganites.

1. INTRODUCTION

Doped perovskite manganites [1], $A_{1-x}A'_xMnO_3$ (A = trivalent La, Pr, Nd, Sm; A′ = divalent Ca, Sr, Ba, Pb), exhibit a complex phase behavior [2] (Fig. 1) and rich physics that arise from the intimate coupling between charge, spin, and lattice degrees of freedom. Of particular interest is the competition between ferromagnetic double exchange and charge-ordering which leads to distinct ground states with increasing doping (x), ferromagnetic (FM) metallic and antiferromagnetic (AF) charge-ordered insulating. For FM compositions and temperatures near the Curie transition (T_C, an insulator-metal transition and colossal magnetoresistance (CMR) are observed. These phenomena have attracted considerable attention [3].

The parent compound, $AMnO_3$ ($Mn3^+$; $t_{2g}^3e_g^1$) is an antiferromagnetic insulator. Hund's rule coupling dictates a $S = 3/2$ t_{2g} localized spin and alignment of the e_g electron spin to make $S = 2$. In octahedral coordination, Mn^{3+} is Jahn-Teller active, thus resulting in a distortion of the MnO_6 octahedra and a distorted perovskite structure [4]. Divalent substitution for A^{3+}, in the simplest picture, converts x Mn^{3+} ions to Mn^{4+}. The latter has spin 3/2 (the t_{2g} core) and is not Jahn-Teller active. Charge transport may be viewed as occurring by transfer of e_g holes on Mn^{4+} to e_g states on neighboring Mn^{3+}. This ''formal valence'' picture of the doped material's electronic configuration, which ignores possible variations in the oxygen stoichiometry in real materials, appears to be an adequate description of the $La_{1-x}Ca_xMnO_3$ system for $x \geq 0.2$ [6].

The starting point for the theoretical description of the ferromagnetic ground state is the double-exchange (DE) mechanism [5]. Due to the strong intra-atomic Hund's coupling, the transfer of e_g holes is inhibited when the spins of the two Mn ions are antiparallel, and in general has an amplitude that is modulated by the factor cos ($\theta/2$), where θ is the angle between the semiclassical directions of the core spins. Thus the hole motion produces partial alignment of the ionic spins, and DE qualitatively explains the occurrence the insulatormetal transition and large magnetoresistance values due to field-induced spin alignment. Theoretical analyses [7] indicated that DE alone is insufficient to account for CMR, and that the electron-phonon interaction plays a supporting role. Numerous experiments now support this view; the electron–phonon interaction contributes through the formation of small polarons in the paramagnetic (PM) phase at $T > T_C$ and in the transition from polaronic insulator to band metal at $T \ll T_C$.

The charge-ordered ground state [8] is one of the more interesting manifestations of the Jahn-Teller interactions in these materials. Below T_{CO} the charge carriers become localized at specific sites, displaying long-range order. The Mn^{3+} e_g orbitals (d_{z^2}) and the associated lattice distortions due to elongated Mn–O bonds also develop long-range order (orbital ordering). Both the carrier localization and structural dis-

[1]Department of Physics, University of Miami, Coral Gables, Florida 33124.

0896-1107/00/0400-0291$18.00/0

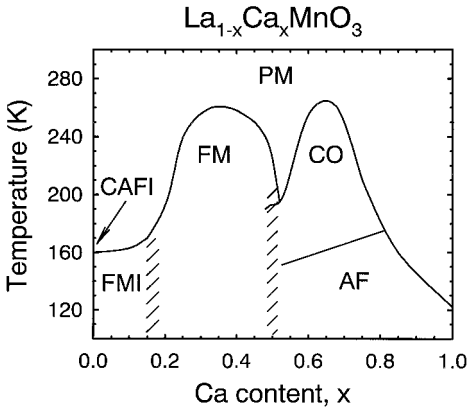

Fig. 1. Schematic phase diagram for $La_{1-x}Ca_xMnO_3$ showing the temperature and doping range of the paramagnetic (PM), ferromagnetic metallic (FM), antiferromagnetic (AF), charge-ordered (CO), ferromagnetic insulating (FMI), and canted antiferromagnetic insulating (CAFI) phases (adapted from Ref. 2).

tortions have a strong influence on transport properties.

Heat in the manganites is carried primarily by the lattice due to the low carrier density, thus studies of thermal conductivity provide insight into the influence of the various phase transitions on the lattice transport. The lattice thermal conductivity is an interesting probe in these compounds because it is quite sensitive to local structural distortions.

We review charge and heat transport in separate sections. Our discussion of charge transport is organized according to the phase diagram, with subsections examining the PM polaronic state, which exists at high temperatures for all doping levels, and the FM and charge-ordered (CO) AF phases, respectively. The final subsection on charge transport addresses CMR compounds for which manipulation of the *A*-site ionic size by substitution yields suppressed values of T_C and the largest magnetoresistance; recent developments suggest that such materials are two-phase mixtures of FM and CO microdomains manifesting percolation physics in their transport. The final section addresses heat transport.

2. CHARGE TRANSPORT

2.1. Paramagnetic State

Transport in the high-temperature, paramagnetic state is well described by small-polaron theory [9] in the regime of thermally activated hopping ($T \gtrsim \hbar\omega_0/k_B$, where ω_0 is an optical phonon frequency). A constant carrier density and activated mobility, $\mu \propto (1/T)\exp(-W/k_BT)$ ($E_P \equiv 2W$ is the polaron binding energy) are characteristic of this regime, and thus the temperature dependencies of transport coefficients are uniquely distinguishable from those of band or disordered semiconductors. In the adiabatic limit, where the electronic motion is assumed to be much faster than that of the lattice, the expressions for electrical conductivity and thermoelectric power are,

$$\sigma(T) = (\sigma_0/T)\exp(-E_\sigma/k_BT)$$

$$S(T) = \left(\frac{k_B}{e}\right)\left(\frac{E_s}{k_BT} + C\right) + \left(\frac{k_B}{e}\right) ln\left(\frac{2S_1+1}{2S_0+1}\right) \quad (1)$$

The thermopower reflects only the energy difference, ε between occupied and unoccupied lattice-distorted sites,[11] and thus its activation energy is smaller than that of the conductivity by amount $W \gg \varepsilon$. Hence a signature of small-polaron transport at high-T is $E_\sigma \gg E_S$. The second term in the thermopower is determined by the configurational entropy of placing a hole with spin S_1 among sites with spin S_0. As discussed above, for hole-doped manganites we have $S_1 = 3/2$ and $S_0 = 2$, so this term is $-19.2\ \mu$V/K.

Figure 2(a) shows E_σ and E_S as functions of doping for LCMO data on polycrystals [12,14–16] and films [11,18,19]. There is quite good agreement between the various sets of specimens. The polaron binding energy, $E_P \simeq 2(E_\sigma - E_S)$, is plotted as a function of doping in Fig. 2(b). A decrease in the polaron formation energy is to be expected as the polaron density increases and they begin to overlap [20]. In addition, the charge of the $La_{1-x}Ca_x$ sublattice decreases with increasing *x,* and this may alter the energy associated with a polaronic lattice distortion [19].

Another interesting issue is the behavior of the prefactor in the conductivity expression, σ_0. Emin and Holstein [9] found, in the dilute limit of noninteracting polarons, $\sigma_0 = 3ne^2a^2\nu/2k_B$, where n is the polaron concentration, a is the intersite hopping distance, and ν is the hopping attempt frequency, i.e., the frequency of a longitudinal optical phonon. The doping behavior of σ_0 in LCMO reported by Worledge *et al.* [19] demonstrates the importance of polaron–polaron interactions in manganite transport. The authors note that the first-order effect is on-site Coulomb repulsion, which dictates an additional factor $1 - x$ in the mobility to account for the probability that an adjacent site is vacant. Since $n = x/a^3$,

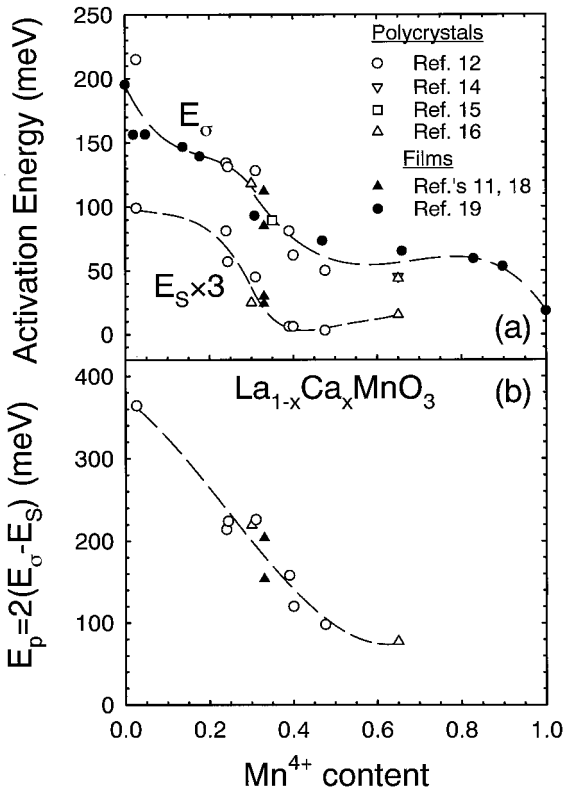

Fig. 2. (a) Doping behavior of the activation energies extracted from electrical conductivity and thermopower vs temperature for $La_{1-x}Ca_xMnO_3$ polycrystals and films using the adiabatic small-polaron model [Eq. (1)]. (b) Doping behavior of the polaron binding energy for LCMO computed from the data in (a).

they propose a modified prefactor, $\sigma_0 = (3ne^2a^2\nu/2k_B)x(1-x)$, and their plot of $a\sigma_0/\nu$ vs x (Fig. 3) agrees qualitatively with this expression at low and high doping where $\sigma_0 \to 0$. The difference between this simple expression and the experimental results may indicate the importance of higher-order terms in the polaron-polaron interactions.

In principle, the high-temperature limit of the thermopower (with the spin-entropy term subtracted), $S_\infty = (k_B/e)C = 86.3C\ \mu V/K$, should provide a measure of the polaron concentration. At high temperatures ($k_BT > E_S$) the thermopower should be given by the Heikes formula [10], $S_\infty = (k_B/e)\ ln[(1-p)/p]$, where p is the number of holes per active transport site. Hundley and Neumeier [12] found $S_\infty \approx 0$ for LCMO polycrystals with $0.18 < x < 0.45$, implying $p \approx 0.5$ independent of the divalent doping level. This result indicates that there are far more holes present and/or far fewer active transport sites than expected based on the nominal valence. They explored a charge disproportionation model wherein Mn^{3+} pairs disproportionate into Mn^{2+}–Mn^{4+} pairs. For transport in such a system the relevant hops are between 2+/3+ and 3+/4+ pairs, and the former are assumed to occur with substantially smaller probability given the 50% larger ionic size difference that should contribute to a much larger polaron hopping energy. Thus Mn^{2+} sites are assumed to be blocking sites for polaron transport. This model fits the observed values of S_∞ quite well.

In spite of this apparent success, the charge disproportionation picture finds little other experimental support. Recent x-ray absorption [6] and x-ray absorption fine-structure (XAFS) [13] studies show little evidence for charge states other than Mn^{3+} and Mn^{4+}, with a smooth evolution with doping from $LaMnO_3$ to $CaMnO_3$. Nevertheless the investigation of Ref. 12 suggests that alternative scenarios in which some sites are rendered inactive may be relevant to explaining the half-filled nature of the thermopower. One possibility, suggested by Jaime *et al.* [18], is that the polarons are in a multiatomic state such that the only active Mn transport sites are those coupled to a divalent dopant. This picture was suggested by the high-T Hall measurements of the authors, which we now discuss.

The T dependence of the Hall coefficient (R_H) in the PM state is also indicative of small-polaron transport. Jaime *et al.* [18] investigated $(La_{1-x}Gd_x)_{0.67}Ca_{0.33}MnO_3$ films, where Gd substitution for La reduces T_C (from 260 K to 145 K for $x = 0.25$), thus increasing the temperature range over which the PM state is experimentally accessible up to $4T_C$. The key

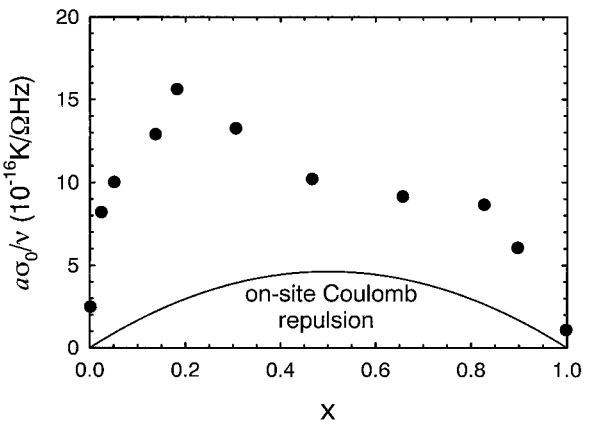

Fig. 3. Doping behavior of the electrical conductivity prefactor (scaled by the ratio a/v; see text) for $La_{1-x}Ca_xMnO_3$ films from Ref. 19.

observations (Fig. 4) for R_H were Arrhenius behavior with activation energy $E_H \approx (2/3)E_\sigma$, and a negative sign in spite of the hole-like behavior indicated by the doping level and thermopower. The theory of the Hall effect for adiabatic small polarons [21] was developed for a triangular lattice, and Jaime *et al.* [18] have extended the theory for a square lattice with hopping (in a plane normal to the applied magnetic field) to nearest neighbors with transfer matrix element $J < 0$ and next-nearest neighbors with reduced transfer energy γJ. The Hall effect in hopping conduction arises from a current induced by the Aharonov-Bohm phase, $\phi = 2\pi\Phi/\Phi_0$, due to the flux Φ proportional to the area enclosed by the hopping trajectory. A sign anomaly occurs when the hopping trajectories involve an odd number of sites [22]. The authors found that both experimental observations agree with the predictions of the modified theory.

Quite recently, Chun *et al.* [23] identified a crossover in the behavior of $R_H(T)$ in a $La_{0.7}Ca_{0.3}MnO_3$ crystal, that appears to signal the breakdown of the small-polaron exponential behavior as the PM–FM transition is approached. The crossover is manifested below $T \simeq 1.4T_C$ as a departure of the activation energies for both $\sigma(T)$ and R_H from their small-polaron values, E_σ and $E_H \approx 2E_\sigma/3$, respectively, at higher T (Fig. 5).

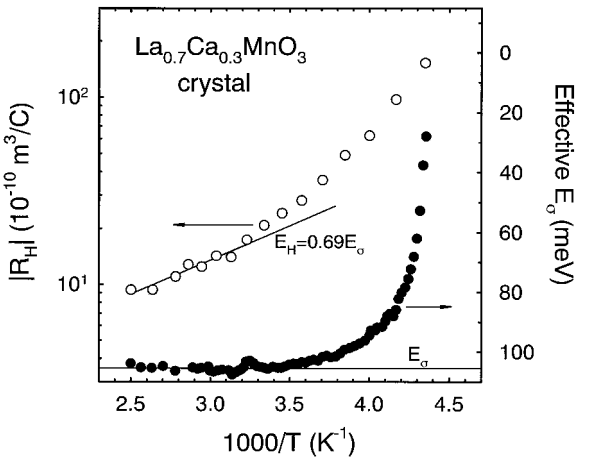

Fig. 5. R_H and ρ_{xx} vs $1/T$ for a $La_{0.7}Ca_{0.3}MnO_3$ crystal showing deviations from their small-polaron activated behavior near 300 K $\simeq 1.4T_C$ [Ref. 23].

2.2. Ferromagnetic state

Let us first discuss transport in the low-temperature limit ($T \ll T_C$), far from the metal-insulator transition where the intrinsic character of the ground state is presumably manifested. The transition regime, $T \simeq T_C$ is treated in the following subsection.

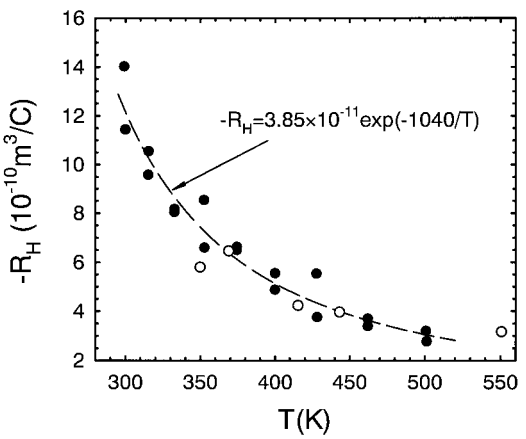

Fig. 4. Hall coefficient vs T in $(La_{1-x}Gd_x)_{0.67}Ca_{0.33}MnO_3$ films for $x = 0$ (open circles) and $x = 0.25$ (filled circles). From Ref. 18.

Several groups [24–26] have identified a correlation between resistivity and magnetization. Hundley *et al.* observed that the phenomenological expression, $\rho(H, T) = \rho_0 \exp[-M(H, T)/M_0]$ represented their data over a wide range of temperatures. Snyder *et al.* [27] have observed a low-temperature behavior ($T/T_C \lesssim 0.5$), $M = M_0(1 - \alpha T^2)$ with α largely independent of field. These authors note that inserting this form in the exponential and expanding yields a resistivity of the form $\rho = \rho_0 + A_2T^2 + A_4T^4$ with both A_2 and A_4 field dependent. Others [2,28,29] have employed similar expressions to fit the low-temperature resistivity. Significantly, Snyder *et al.* found experimentally that A_2 is independent of field. They argue that the power-law expression, with field-independent T^2 term is thus a more appropriate description than the exponential at low temperatures. However, near T_C in the CMR regime the exponential behavior provides a better description and we return to this in the next section.

The field-independent T^2 term has been attributed to electron-electron scattering. The ratio A_2/γ^2 (γ is the electronic specific heat coefficient) is 60–70 times the Kadowaki-Woods [30] value of 1×10^{-5} $\mu\Omega$ cm (mole K/mJ)^2 that typifies heavy-fermion materials, and more than 600 times larger than values found for transition metals [29,44]. Jaime *et al.* [29] interpret this as a strong argument against attributing the T^2 term to electron-electron scattering. Instead, these authors observed a correlation between the coefficient

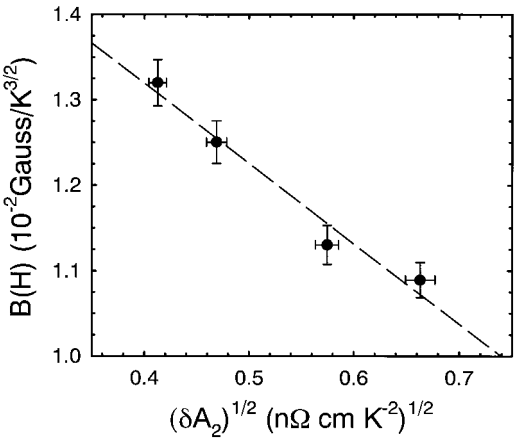

Fig. 6. Coefficient B from $T^{3/2}$ term in low-T magnetization vs $\sqrt{\delta A_2}$, where δA_2 is the field-induced change in the coefficient of the T^2 term in resistivity, for a $La_{0.66}(Pb_{0.67}Ca_{0.33})_{0.34}MnO_3$ crystal [29].

of the $T^{3/2}$ term in M(T) and $\alpha(H)$ for $La_{0.66}(Pb_{0.67}Ca_{0.33})_{0.34}MnO_3$ crystals that they interpret as evidence that A_2 is determined by one-magnon scattering.

In a ferromagnetically ordered, half metallic system at low temperatures, there are no minority-spin states available for conduction, and thus electron-magnon scattering, which involves a spin-flip transition, is not possible. At higher temperatures, local spin disorder effectively introduces minority-spin states and the magnon scattering channel is turned on with characteristic T^2 term in $\rho(T)$. This scenario implies a constant resistivity at the lowest temperatures, due to scattering by static disorder, and T^2 behavior at intermediate temperatures as observed experimentally [29].

The low-temperature magnetization of their crystals behaved as expected in the spin-wave approximation, $M(T) = M(0) - BT^{3/2} - \cdots$, with a stiffness constant $D = 165$ meV Å^2, in agreement with neutron scattering measurements [31]. Application of a magnetic field introduces a gap in the magnon spectrum given by the Zeeman energy, $\Delta = g\mu_B H$, such that $B(H) \approx B(0)(1 - 1.36\sqrt{\Delta/k_B T} + \cdots)$. Their extension of the one-magnon scattering theory of Mannari [32] to incorporate a small shift in the Fermi momentum for minority- and majority-spin subbands implies $A_2(0)-A_2(H) \equiv \delta A_2 \propto \Delta/k_B T$. That $B(H)$ is approximately linear in $\sqrt{\delta A_2}$ (Fig. 6) is consistent with a T^2 resistivity term arising from one-magnon scattering.

The Hall coefficient also gives some insight into the electronic structure of the FM phase. In ferromagnetic metals, the asymmetric (skew) scattering of transport charges from magnetic moments gives rise to a transverse voltage (*anomalous* Hall effect, R_s) that adds to the *ordinary* Hall effect (R_H) associated with the Lorentz force, resulting in a transverse resistivity [39],

$$\rho_{xy} = R_H[\mu_0 H + \mu_0(1 - N)M] + R_s\mu_0 M \qquad (2)$$

where N is the demagnetization factor. A typical behavior of $\rho_{xy}(B)$ is shown in the inset of Fig. 7 (that R_s is opposite in sign to R_H is unusual and discussed further below). The available data [33–38] all indicate a Hall density, $n_{eff} = V_{f.u.}/R_H e$ ($V_{f.u.}$ is the formula unit volume), substantially larger than the nominal doping level would imply, with values ranging from 0.85–2.4 holes/Mn. Representative data [36,38] for $n_{eff}(T)$ are shown in Fig. 7. These groups interpret the large value of n_{eff} to be evidence for compensation, as indicated by the band structure and virtual crystal calculations of Pickett and Singh [40]. The calculations indicate two majority-channel Fermi surfaces (FS's): a Γ-centered sphere containing 0.05 electrons/Mn, and an R-centered cube containing 0.55 holes/Mn. Chun *et al.* [38] note that, given the very low mobility of the manganites, the Hall experiments probe the low-field limit where a dimensionless factor (r) must be included for non-spherical FS's. Thus in a two-band model, $R_H = (r_h n_h \mu_h^2 - r_e n_e \mu_e^2)/[e(n_h\mu_h + n_e\,\mu_e)^2]$. Assuming $\mu_h = \mu_e$ and taking [41] $r_h = 1/2$ for the cubic

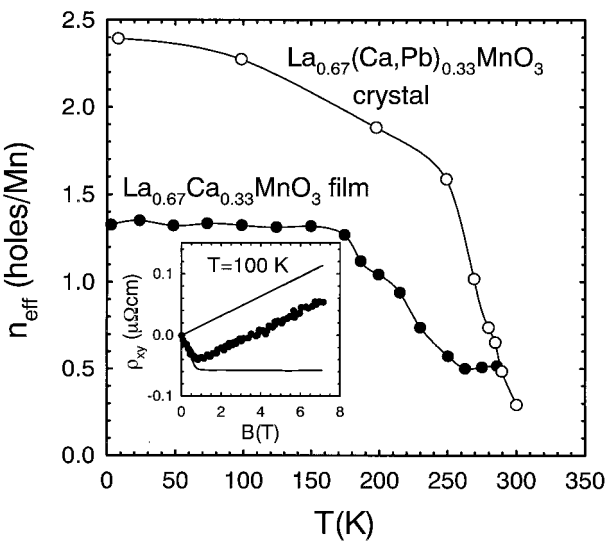

Fig. 7. Hall number vs T for a $La_{0.67}Ca_{0.33}MnO_3$ film [36] and $La_{0.66}(Pb_{0.67}Ca_{0.33})_{0.34}MnO_3$ crystal [38]. The inset shows ρ_{xy} vs B for the crystal at 100 K, demonstrating the decomposition into ordinary and anomalous contributions.

FS yields, n_{eff} = 1.6 holes/Mn. Allowing different carrier mobilities can bring the calculations into agreement with experimental values. Jakob *et al.* [36] also noted variations in the experimental value of n_{eff} ranging from 1.1 to 1.9 holes/Mn for several films grown under nominally the same conditions, thus suggesting that these variations are associated with slight differences in stoichiometry as might be expected for a compensated material.

Asamitsu and Tokura [37] investigated the low-temperature behavior of R_s (a discussion of R_s near T_C is presented in the next section). They found two approximate empirical scaling relations, $-R_s \propto \rho_{xx}^{\alpha}(\alpha \simeq 1.2\text{–}2$ depending on doping and temperature range) and $R_s = -1.3 \times 10^{-9}$ Ω cm/G $[M(0) - M(T)]^{3/2}$, with M in units μ_B/Mn. Chun *et al.* [38] reported $-R_s \propto \rho_{xx}$ for $T < 270$ K in a $La_{0.66}(Pb_{0.67}Ca_{0.33})_{0.34}MnO_3$ crystal ($T_C \approx 300$ K), and more recently [23] observed $-R_s \propto \rho_{xx}^2$ for $T < 200$ K in a $La_{0.7}Ca_{0.3}MnO_3$ crystal ($T_C = 216$ K). The relation $R_s \propto \rho_m^2$ (ρ_m is the resistivity caused by magnetic scattering) is known from conventional ferromagnets [39] but the sign of R_s, the other power laws, and the absence of a peak in R_s below T_C are inconsistent with existing theory [41,42]. The values of R_s for the manganites are an order of magnitude smaller than that of Ni[43] for comparable values of ρ_{xx} (~100 $\mu\Omega$ cm).

The doping behavior of the transport coefficients in $La_{1-x}Sr_xMnO_3$ has been reported by Okuda *et al.* [44]. Interestingly, their data indicate that lattice effects play a role, particularly as the doping-dependent insulator-metal transition (near $x = 0.17$) is approached from above. They observed (Fig. 8) an enhancement of the T^2 resistivity coefficient, residual resistivity, electronic and lattice specific heat that coincide with a suppression of the Hall coefficient [37] for $x < 0.30$. The small value of the Hall coefficient indicates that a large FS is maintained down to the MI transition. The lattice softening suggests that the dynamically orbital-ordered or Jahn-Teller distorted background plays an increasingly important role in the charge dynamics of the fully spin-polarized carriers as the MI boundary is approached. For example, it implies that the interpretation of Jaime *et al.* for the origin of the T^2 term in resistivity at $x = 0.33$ may be only part of the story for compositions closer to the metal-insulator boundary.

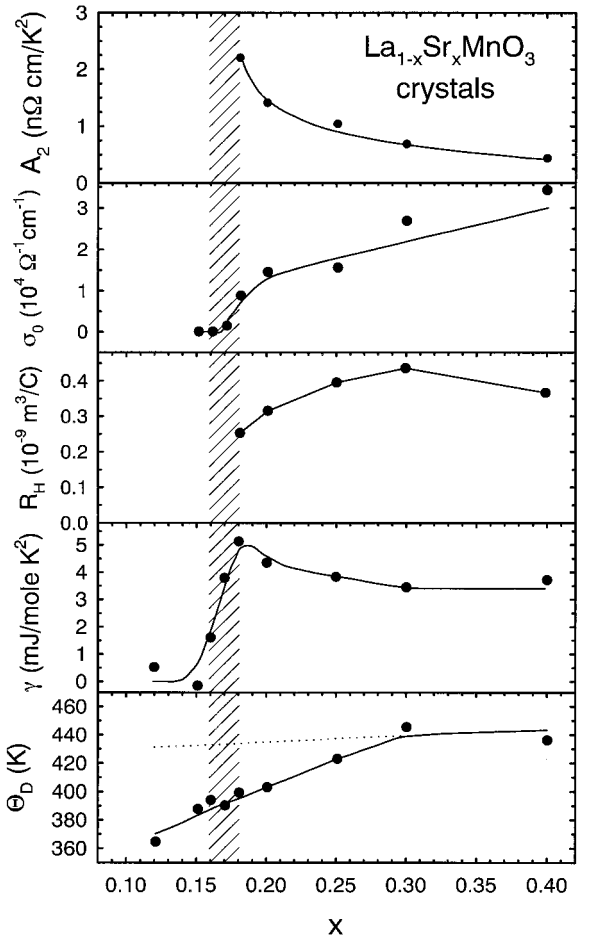

Fig. 8. Doping behavior of the T^2 term in resistivity (A_2), inverse residual resistivity (σ_0), Hall coefficient, electronic specific heat coefficient (γ), and Debye temperature for LSMO from Ref. 44.

2.3. PM-FM Transition Region

In the temperature range near T_C and the insulator-metal transition the physics governing transport in the manganites is least understood. A coexistence of polaronic and itinerant carriers is likely, and an effective medium analysis gives reasonable agreement with the temperature and field dependencies of transport coefficients [45].

The most prominent feature of transport in this regime is the insulator-metal transition that coincides with T_C and is characterized by a colossal magnetic field [46] (CMR) and pressure-dependent [47,48] resistance (Fig. 9). Both effects are qualitatively understood to arise from an increase in the effective transfer integral (bandwidth), $t_{eff} = t_0\cos(\theta/2)$, with pressure primarily increasing the bare hopping term t_0, and field aligning the spins (decreasing θ).

As noted in the preceeding section, an exponential correlation between resistivity and magnetization has been noted by several authors [24–26]. Hundley

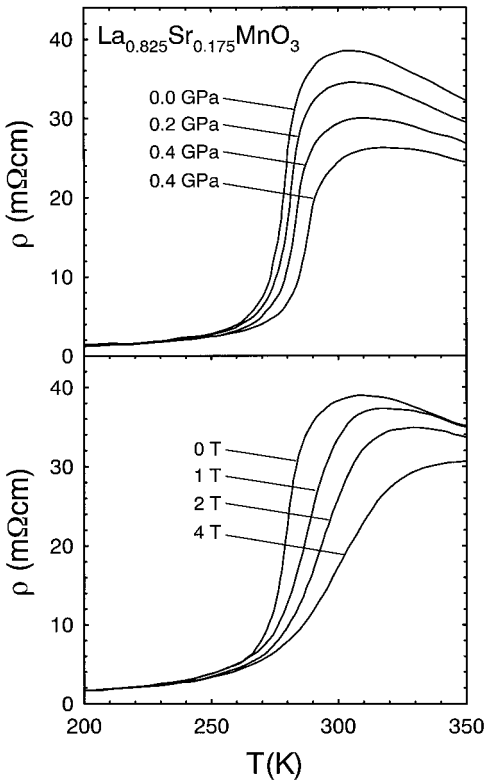

Fig. 9. Electrical resistivity *vs* temperature near T_C at various (a) hydrostatic pressures and (b) magnetic fields for a $La_{0.825}Sr_{0.175}MnO_3$ single crystal from Ref. 47.

et al. [25] found $\rho(H, T) = \rho_0 \exp[-K_\rho M(H, T)/M_0]$, with $K_\rho = 5.2 \pm 0.3$ for a $La_{0.7}Ca_{0.3}MnO_3$ film (Fig. 10). They note this correlation is consistent with polaronic charge transport, $\rho \sim \exp(-t_{eff})$, with the temperature and field-dependent magnetization, $M(H, T)$, a measure of t_{eff} as dictated by the double-exchange mechanism. Cohn *et al.* [17] observed a similar behavior near T_C for a $La_{0.83}Sr_{0.17}MnO_3$ single crystal, with $K_\rho = 4.7$.

Interestingly, the XAFS measurements of Booth *et al.* [13] reveal a correlation between MnO_6 distortions and magnetization that is similar to the exponential relationship, $\rho(M)$, suggested from the transport data. The data were analyzed within a "two-fluid" picture wherein it is assumed that in the FM state the polaronic distortions observable above T_C are removed around a fraction of the Mn sites with the creation of a delocalized hole at each site. The delocalized hole concentration, n_{dh}, for several LCMO compositions (Fig. 11) was found to obey the relation, $n_{dh} = n_0(x) \exp[K_n (M/M_0 - 1)]$, with $n_0(x) = 0.16, 0.19, 0.26$ for $x = 0.21, 0.25, 0.30$, respectively, and $K_n = 3.8 \pm 0.2$. Booth *et al.* [13] noted that, since $\rho = 1/ne\mu$, the discrepancy between the coefficients K_n and K_ρ could imply that the mobility is also exponentially dependent on M, $\mu = \mu_0 \exp(K_\mu M/M_0)$, with $K_\mu = 1.4 \pm 0.4$.

Of particular interest are recent studies of the anomalous Hall effect in the transition regime. Matl *et al.* observed a correlation between R_s and the zero-field longitudinal resistivity [Fig. 12(a)], $R_s(T) = \alpha(0)\rho_{xx}(T)$, with $\alpha = 3.3 \times 10^{-4}$ m^2/Vs at $T \geq 200$ K for a $La_{0.67}Ca_{0.33}MnO_3$ film ($T_C = 265$ K). From (2) above in the limit $H \to 0$, this implies $\tan\theta_H \equiv \rho_{xy}/\rho_{xx} = \mu_o \alpha \chi H$ where χ is the magnetic susceptibility. Interestingly they observed that the inverse Hall mobility, $1/\mu_H \equiv B/\tan\theta_H$, is field independent for fields less than H_p, and rises sharply for $H > H_p$ [Fig. 12(b)] (the increase in H_p with T follows that of $1/\chi$). These

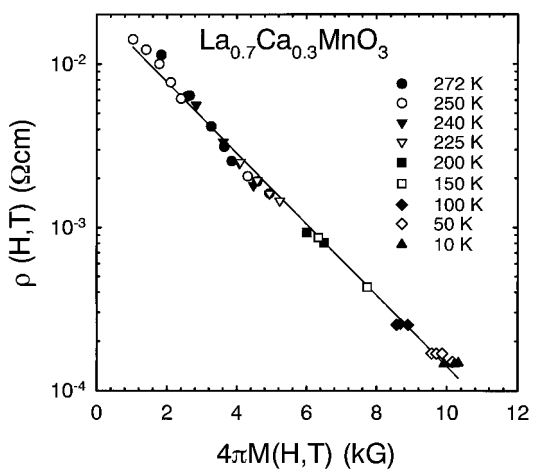

Fig. 10. Electrical resistivity for a $La_{0.7}Ca_{0.3}MnO_3$ film plotted vs magnetization at various temperatures from Ref. 25.

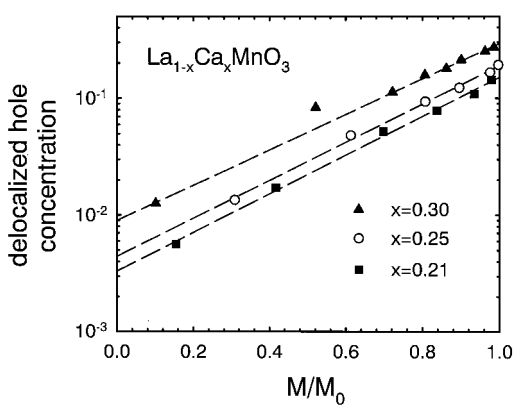

Fig. 11. Concentration of delocalized holes inferred from XAFS measurements and a "two-fluid" model plotted vs the normalized magnetization from Ref. 13.

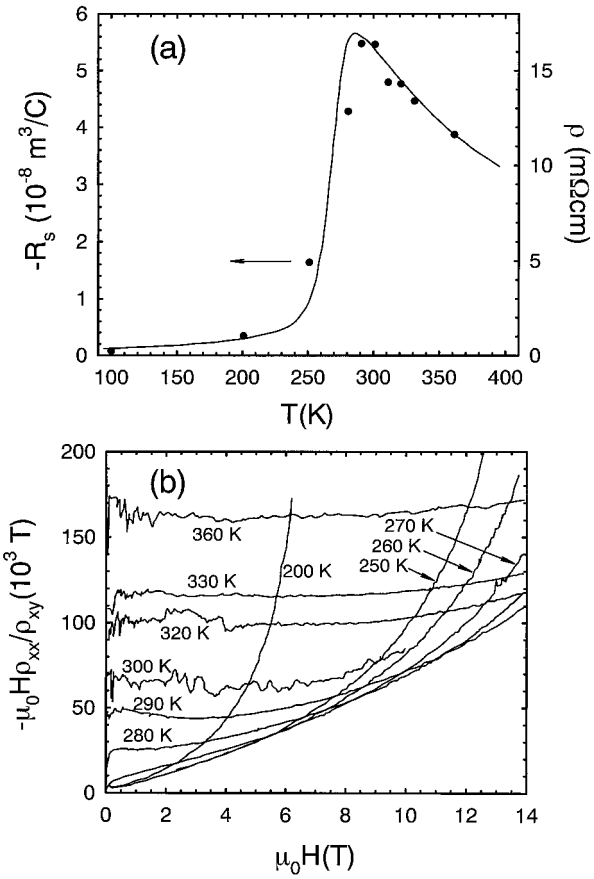

Fig. 12. (a) Anomalous Hall coefficient, R_s, and zero-field longitudinal resistivity near T_C for a $La_{0.67}Ca_{0.33}MnO_3$ film from Ref. 35. (b) inverse Hall mobility vs magnetic field at various fixed temperatures for the same film.

results are surprising given that ρ_{xx} is strongly field dependent in this regime, and suggests that CMR is driven by a field-induced change in mobile carrier density rather than by a change in scattering rate.

These data stimulated theoretical investigations [49–51] into the problem of the anomalous Hall effect for hopping conduction with double exchange. In this situation the spin of a hopping hole is constrained to be anti-aligned with the core spin at each of the sites along a hopping trajectory; the problem is reduced to a triad of sites as in the case of the ordinary Hall effect treated by Holstein (see above) [21]. Though there is a net magnetization of the core spins, thermal fluctuations yield inhomogeneous spin configurations, particularly near T_C. The hopping hole accumulates a phase related to the sequence of its spin states as it moves from site to site. Returning to a site returns its spin state, but interference with other trajectories occurs due to their differing phases. The presence of the spin-orbit interaction ensures that a particular sense of carrier circulation on the triad will be favored for a given core-spin configuration, so that the anomalous Hall current does not average to zero upon averaging over core-spin configurations [50].

Viewing the system near T_C as a small-polaronic background with conducting ferromagnetic inclusions, the recent Hall experiments of Chun *et al.* [52] motivate the plausible assumption that the conducting network is composed of triads with core spins oriented roughly along the average magnetization. This assumption dictates a simplified core-spin angular distribution related to the ratio $m(H, T) = M(H, T)/M_{sat}$ and thus the Anderson-Hasegawa [5] factors $\cos^2(\theta/2)$, which appear in the hopping probabilities, can be computed to yield ρ_{xy} that depends only on H and T through $m(H, T)$. The corresponding curve is shown in Fig. 13 in good agreement with experimental data for $T \geq T_C$.

2.4. Charge Ordered State

For doping concentrations $x \geq 0.5$, Mn^{3+} and Mn^{4+} ions in LCMO form ordered superlattices, and the ground state is antiferromagnetic (Fig. 1). Electron microscopy and neutron diffraction studies [53–55] indicate that the charge-ordered state is also orbitally ordered. The most dramatic effects in

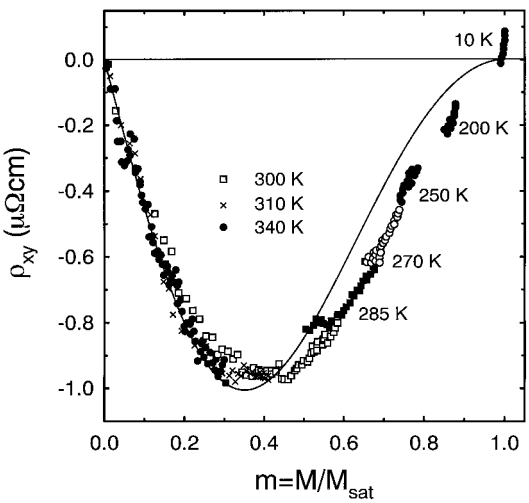

Fig. 13. Hall resistivity vs magnetization for a $La_{0.66}(Pb_{0.67}Ca_{0.33})_{0.34}MnO_3$ crystal from Ref. 52. The solid curve is $\rho_{xy} = -4.7$ $\mu\Omega$ cm $[m(1 - m^2)^2]/[(1 + m^2)^2]$ as derived from the theory of Ref. 50.

transport are seen for $x = 0.5$, but charge and orbital ordering occur at other doping concentrations as well, particularly for compositions for which the superstructures have modulation wavelengths that are commensurate with the lattice, as in $La_{5/8}Sr_{1/8}MnO_3$ [56]. The charge and orbital ordering patterns for some of the compositions are depicted in Fig. 14.

Kuwahara *et al.* [57] have investigated the transport and magnetic properties of the half-doped system $(Nd_{1-y}Sm_y)_{1/2}Sr_{1/2}MnO_3$ ($0 \leq y \leq 1$). The Sm doping allows fine tuning of the tolerance factor $f = (\langle r_A \rangle + r_O)/[\sqrt{2}(r_{Mn} + r_O)]$, where $\langle r_A \rangle$, r_{Mn}, and r_O are the averaged ionic radii of the A-site, Mn and O ions, respectively. f controls the deviation of the Mn–O bond angles from 180° and thus the one-electron bandwidth through the e_g-electron hopping integral [58,59]. Upon cooling from 300 K the half-filled materials undergo a ferromagnetic transition, followed by the CO transition. Representative data for $y = 0.25$ are shown in Fig. 15. Application of a magnetic field stabilizes the ferromagnetic phase to lower temperatures, completely destroying the charge order for $H \geq 6$T.

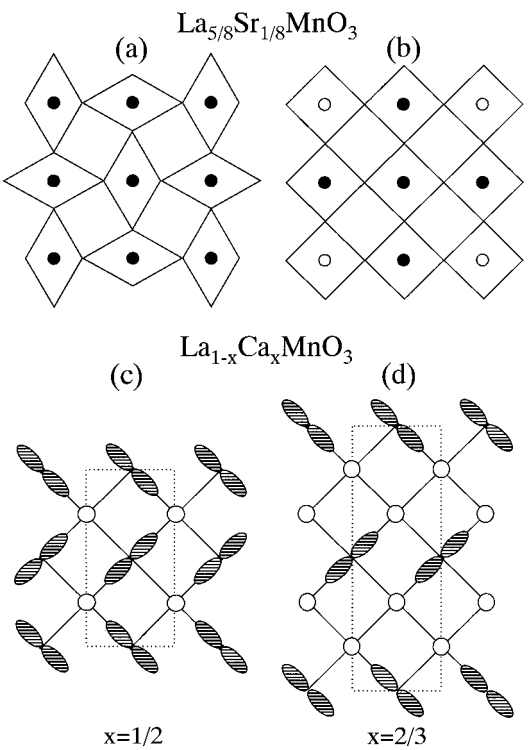

Fig. 14. Depiction of the charge and orbital ordering pattern in the *ab*-planes of $La_{7/8}Sr_{1/8}MnO_3$ (from Ref. 56) with alternating Mn–O planes along the *c*-axis composed of (a) cooperatively ordered Jahn-Teller-distorted Mn^{3+} ions (solid circles) and (b) Mn^{4+} holes (open circles) ordered in a less distorted, 1/4-filled lattice. (c) and (d) show the ordering patterns in the *ac*-plnes of $La_{1-x}Ca_x$ MnO_3 for $x = 1/2$ and $x = 2/3$, respectively [54,55]. Hatched lobes represent d_{z^2} orbitals of Mn^{3+} ions (elongated axis of MnO_6 octahedra). Dotted lines show the superstructures.

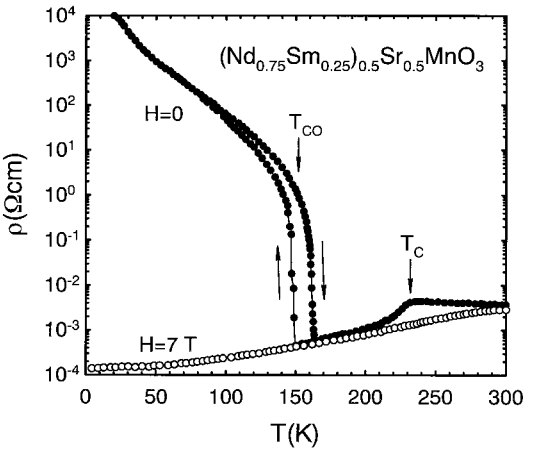

Fig. 15. Electrical resistivity vs temperature for a $(Nd_{0.75}Sm_{0.25})_{0.5}$ $Sr_{0.5}MnO_3$ crystal from Ref. 57.

These observations on the half-doped materials are consistent with expectations that a magnetic field favors ferromagnetism and itinerancy via the DE interaction. However, a study [60] of $La_{7/8}Sr_{1/8}MnO_3$ indicates that T_{CO} actually increases with applied magnetic field (Fig. 16). These authors argue that this different behavior in the lightly-doped manganites reflects the role of cooperative Jahn-Teller distortions which are not present in the higher doping regime ($x \geq 0.5$). Upon cooling from 300 K (in zero

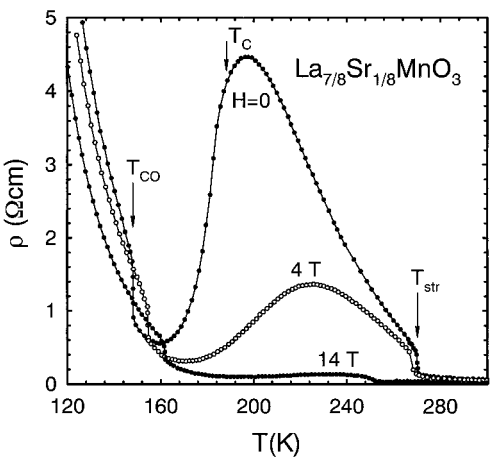

Fig. 16. Electrical resistivity vs temperature for a $La_{7/8}Sr_{1/8}MnO_3$ crystal in various magnetic fields [60].

field) this compound passes through a structural transition ($T_{str} \simeq 270$ K) from orthorhombic to a cooperative Jahn-Teller distorted phase [61], followed by the ferromagnetic ($T_C \simeq 187$ K) and charge-order ($T_{CO} \simeq 150$ K) transitions. These distortions are suppressed by ferromagnetic ordering, as evidenced by the depression of T_{str} in applied magnetic field. In the charge-ordered phase, the application of a magnetic field presumably does not significantly alter the Jahn-Teller energy because the carriers remain localized. Thus the T_{CO} enhancement with field is evidently associated with the decrease of the cooperative Jahn-Teller distortion in the ferromagnetic phase.

2.5. Coexisting FM and CO Phases and Low-T_C Materials

For CMR compounds near optimal doping ($x \approx 0.3$) T_C decreases dramatically with decreasing tolerance factor [58,59], such that it is possible to suppress T_C from $\simeq 265$ K to <100 K. Though a suppression of T_C is to be expected from a reduced bandwidth, there are indications that the change in bandwidth is insufficient to account for the large change in T_C [62]. The nature of the FM state in the low-T_C compounds is also at issue given that the resistivity below T_C is metallic-like in its temperature dependence, but has a magnitude that exceeds the Mott metallic limit.

Zhou *et al.* [63] studied the pressure dependence of the resistivity and thermopower in polycrystalline $(La_{0.25}Nd_{0.75})_{0.7}Ca_{0.3}MnO_3$ (Fig. 17). As in the high-T_C materials, the ferromagnetic transition occurs at a temperature near or somewhat below the maximum in ρ. The thermal hysteresis is characteristic of the transport in such low-T_C materials. The strong pressure dependence of ρ below T_C contrasts with the behavior in the polaronic PM state, and suggests that there is a strong increase in the density of mobile charge carriers with pressure in the FM state. Upon passing below T_C the thermopower decreases abruptly from $\sim$80 μV/K to metallic-like values on the order of 1–2 μV/K. Curiously, the thermopower is independent of applied pressure at $T < T_C$. Zhou *et al.* note that the large values of resistivity in the FM state would suggest a small value of E_F and imply a large linear-T slope for a metallic thermopower, contrary to the nearly T-independent behavior observed. The authors proposed a novel electronic state, involving a vibronic coupling between electrons and phonons, in which holes are condensed into a degenerate state without energy dispersion.

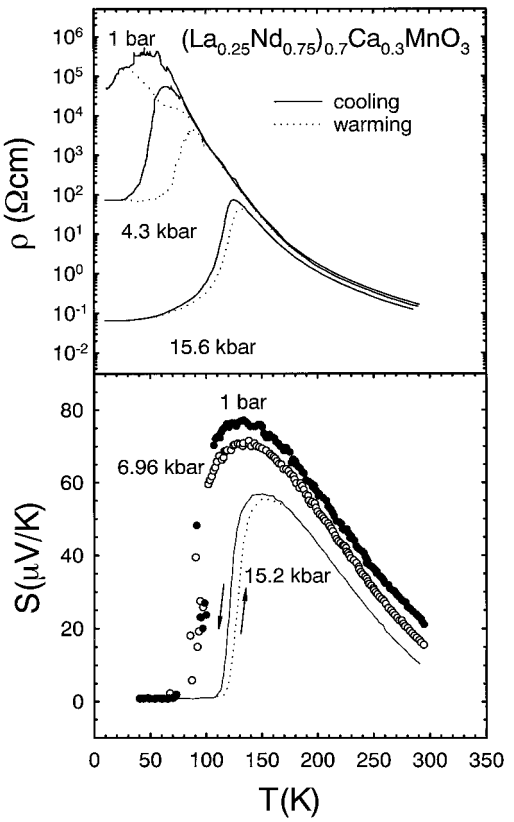

Fig. 17. (a) Electrical resistivity and (b) thermopower vs temperature for polycrystalline $(La_{0.25}Nd_{0.75})_{0.7}Ca_{0.3}MnO_3$ under hydrostatic pressure [63].

Quite recently, Uehara *et al.* [64] reported transport and microscopy studies of the low-T_C materials $La_{5/8-y}Pr_yCa_{5/8}MnO_3$ indicating the coexistence of submicron-sized FM and CO domains over a broad range of compositions. This phase separation is not associated with chemical inhomogeneity, but appears to be a generic consequence of the competing interactions driving the CO and FM states in narrow bandwidth systems for which T_C and the charge delocalization transition are suppressed below the freezing point of Jahn-Teller polarons [65]. They suggest that percolation underlies CMR in the low-T_C compounds. The results are compelling and appear to offer an alternative explanation for the anomalous transport properties observed by Zhou *et al.*

Figure 18(a) shows the resistivity of $La_{5/8-y}Pr_y Ca_{5/8}MnO_3$. For $y \geq 0.3$ the material has a charge-order transition at $T \simeq 210$ K as indicated by the upturn in $\rho(T)$. The FM and CO ground states clearly

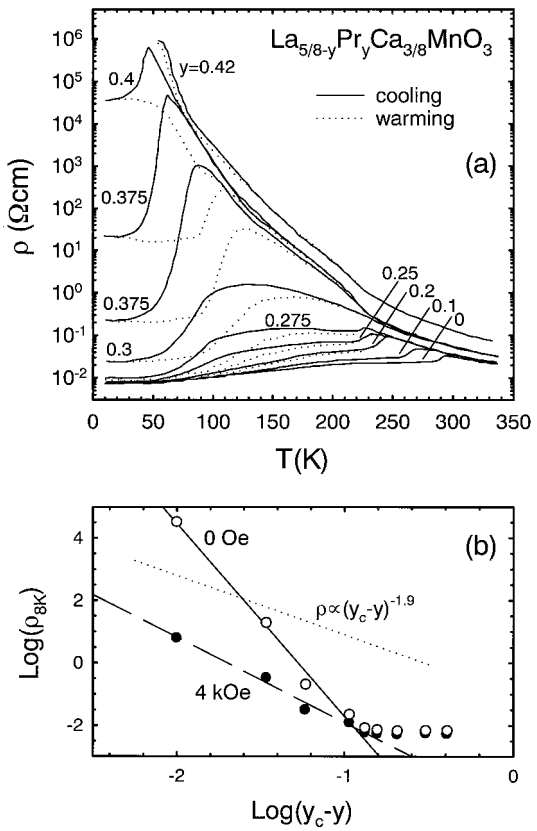

Fig. 18. (a) Electrical resistivity vs temperature for $La_{5/8-y}Pr_y Ca_{5/8}\ MnO_3$ and (b) Log–Log plot of $\rho(8\ K)$ vs $y_c - y$ ($y_c = 0.41$) for zero- and applied magnetic field. The dotted line corresponds to the expectation of classical percolation theory [64].

compete as evidenced in the rather gradual decrease in T_C with increasing y for $y \leq 0.25$, followed by a more rapid decrease for $y \geq 0.3$. To motivate a two-phase scenario for the transport, the authors note that the ratio of the saturation moment at $y = 0.4$ ($\sim$0.6 μ_B) to the full moment ($\sim$4 μ_B) is within the range of percolation thresholds for three-dimensional systems (10–25%). Percolation theory predicts $\rho \propto |y_c - y|^{-1.9}$, and power-law behavior is observed for the low-T ρ in the range $0.275 \leq y \leq 0.4$ (using $y_c = 0.41$), with exponents -6.9 and -2.6 in zero-field and 4 kOe, respectively (Fig. 18(b)). It is suggested that the larger experimental exponents are attributable to the strong sensitivity of the transport in manganites to alignment of FM domains. This presumably explains the reduction of the exponent in applied field. The alignment is likely inhibited as y approaches y_c as the increasing volume fraction of CO domains leads to a poor connectivity of the FM regions. Interestingly, the charge order observed was always of the $x = 1/2$ type (Fig. 14), the phase that is readily converted to FM under applied field.

2. HEAT TRANSPORT

Heat is transported in the manganites predominantly by the lattice at all doping levels and temperatures, and thus studies of thermal conductivity [17,66,67] (κ) offer an opportunity to investigate the influence of coupled charge, spin and lattice degrees of freedom through their effects on long-wavelength heat-carrying phonons.

Thermal conductivity data [17] for a series of polycrystalline LCMO specimens is shown in Fig. 19(a). κ for undoped $LaMnO_3$ is surprisingly low for a crystalline insulator ($\sim$1W/mK), approaching the

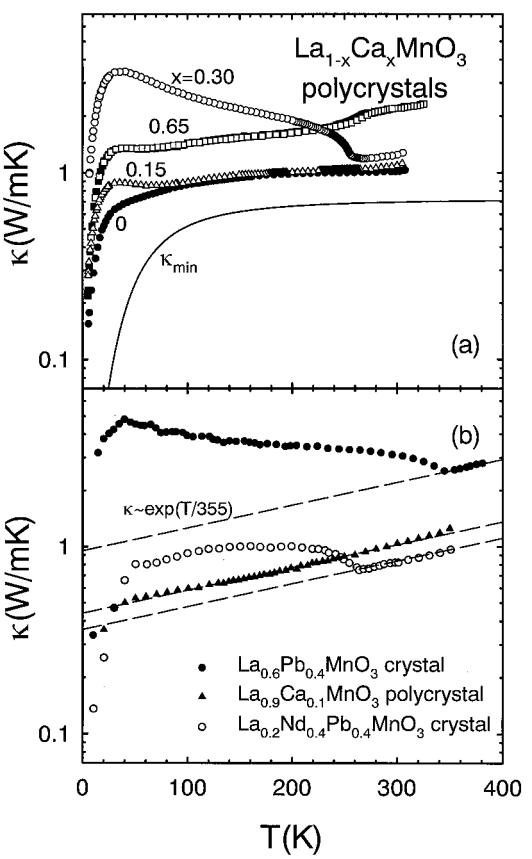

Fig. 19. (a) Thermal conductivity vs temperature for LCMO polycrystals from Ref. 17. The solid line labeled κ_{min} represents the theoretical minimum themal conductivity computed for $LaMnO_3$ using the model of Ref. 68. (b) Thermal conductivity vs temperature for several perovskite manganites from Ref. 67. The dashed lines represent $\kappa \propto \exp(T/350)$.

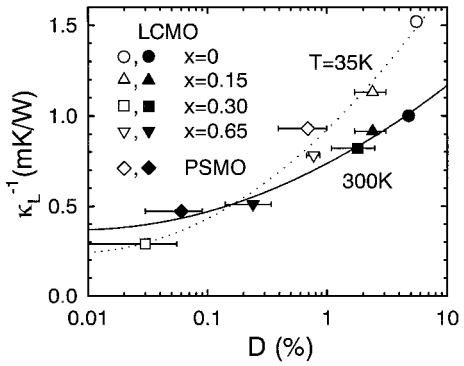

Fig. 20. Lattice thermal resistivity vs Mn-O bond distortion (see text) for manganite polycrystals (Ref. 17).

theoretical minimum value [68] and indicative of a high degree of disorder. Such behavior in crystalline materials is characteristic of random, noncentral distortions of the lattice, and attributable in the manganites to Jahn-Teller distortions of the MnO_6 octahedra.

In the PM phase, Visser *et al.* [67] reported an anomalous temperature dependence [Fig. 19(b)], $\kappa \propto \exp(T/350)$, and motivated by neutron scattering observations of large and T-dependent Debye-Waller factors [69,73] attributed this behavior to dynamical lattice distortions. However for similar compositions, the data of Cohn *et al.* [(Fig. 19(a)] show no such behavior. Radiation losses at $T > 200$ K can be severe and if uncorrected can yield a substantial overestimate of κ with an error that increases rapidly with T—a possible explanation for the discrepancy between the data of the two groups.

Cohn *et al.* [17] have demonstrated (Fig. 20) that the lattice thermal resistivity, $W_L = \kappa_L^{-1}$, correlates with a measure of the bond disorder determined from neutron diffraction, $D \equiv (1/3)\sum_{i=1}^{3} |(u_i - \overline{u})/\overline{u}| \times 100$, with u_i the Mn—O bond lengths, and $\overline{u} = (u_1u_2u_3)^{1/3}$. The correlation is especially compelling because it holds at both high-T and low-T while D is dramatically altered by the ferromagnetic and charge-ordering transitions upon cooling from the PM state. For example, $Pr_{0.5}Sr_{0.5}MnO_3$ has the smallest D at 300 K, but one of the largest at 35 K; the reverse is true for $La_{0.7}Ca_{0.3}MnO_3$. The various phase transitions all involve modifications of the local structure [13,69], which correlate with hole itinerancy and the magnetism, consistent with a polaronic origin for the lattice distortions.

The close correspondence between the lattice and charge transport is further evidenced by the magnetic field dependence of κ. Cohn *et al.* [17] measured $\kappa(H)$ at three temperatures near T_C for a $La_{0.83}Sr_{0.17}MnO_3$ crystal. Using magnetization curves measured on the same specimen they found $W = \kappa^{-1}$ to be a single function of $M(H, T)$, with $\kappa^{-1}(H, T) = A - BM^2(H, T)$ providing a good fit (Fig. 21). The change in the lattice contribution [dashed line, Fig. 21] predominates in the magneto-thermal resistivity. These results indicate that both the lattice and charge mobilities are governed by the same local physics and complement measurements of magnetovolume effects [70,71] which indicate that substantial field-induced structural changes occur in these materials.

Another interesting issue for heat transport studies is how charge ordering influences the damping of heat-carrying phonons [74]. To address this issue it is useful to consider the kinetic theory expression for the lattice thermal resistivity, $W_L = (3/Cv^2)\tau^{-1}$, where C_L is the lattice specific heat, v is the sound velocity, and τ^{-1} is the phonon relaxation rate. Figure 22(a) shows that in the case of $La_{0.35}Ca_{0.65}MnO_3$ the charge ordered phase is characterized by a substantial hardening of the lattice [72], with v increasing by 10% just below T_{CO}. The background lattice specific heat is continuous well above and below T_{CO} and the volume change at T_{CO} is negligible [72] thus the κ data imply a substantial increase in phonon damping (τ^{-1}) below T_{CO}. Figure 22(b) shows $\tau^{-1}(T)$ computed for from the $\kappa(T)$ using $C_L(T)$ and $v(T)$ from Ref. 72 and taking $v(T_{CO}) = 3{,}000$ m/s. Also shown is $\tau^{-1}(T)$ for $La_{0.85}Ca_{0.15}MnO_3$, computed assuming $v = 3{,}000$ m/s independent of T, and scaled to match the data for $x = 0.65$ at $T > T_{CO}$. The $x =$

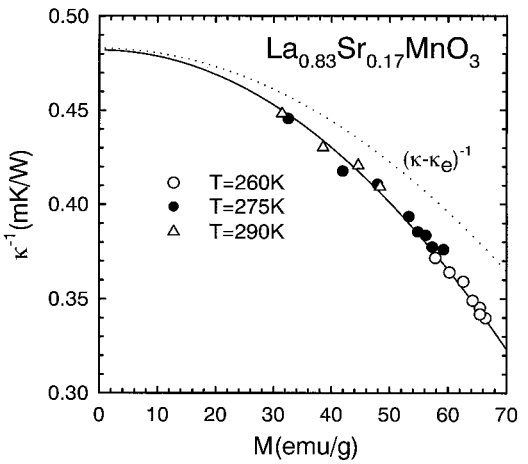

Fig. 21. Lattice thermal resistivity vs magnetization for a $La_{0.83}Sr_{0.17}MnO_3$ crystal from Ref. 17.

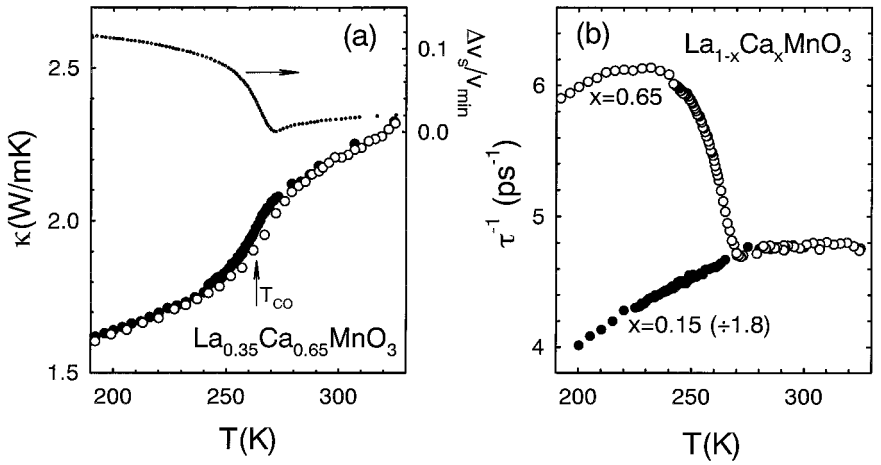

Fig. 22. (a) Thermal conductivity vs temperature for $La_{0.35}Ca_{0.65}MnO_3$ polycrystal [17] along with the relative change in sound velocity [72]. (b) phonon scattering rate vs temperature for $La_{1-x}Ca_xMnO_3$ $x = 0.15$, 0.65, computed as described in the text [74].

0.15 compound remains in the PM phase for $T > 140$ K, and thus serves as a reference for the phonon scattering rate in the absence of charge ordering. $\tau^{-1}(T)$ for $x = 0.65$ increases abruptly by nearly 40% just below the transition, and then decreases at $T <$ 230 K, paralleling the scaled $\tau^{-1}(T)$ for the $x = 0.15$ compound. This constant offset of the $\tau^{-1}(T)$ curves indicates that the enhanced scattering in the CO phase is associated with an abrupt change in the static bond disorder.

It is significant that $\tau^{-1}(T)$ for $La_{0.35}Ca_{0.65}MnO_3$ shows no anomalous behavior at $T > T_{CO}$ whereas $v(T)$ indicates a softening of the lattice, presumably associated with chargeorder fluctuations as T_{CO} is approached from above. Evidently such dynamical bond disorder (presumably with a frequency related to that of an optical phonon involved in polaron hopping) does not necessarily yield damping of heat-carrying phonons.

4. SUMMARY

The transport properties of the perovskite manganites continue to enrich and challenge our understanding of these interesting materials. The FM and PM states governed by double-exchange and Jahn-Teller physics, respectively, appear reasonably well understood, though issues concerning the T-dependent scattering rate in the FM regime and the high-T thermopower remain to be addressed theoretically. There has been progress in developing a better understanding of the complex PM-FM (CMR) transition regime where polaronic and itinerant carriers appear to coexist. The competing interactions which determine the CO and FM states and the general phase behavior appear to dictate a novel phase separation controlling the transport for low-T_C CMR compositions. There is no doubt that further systematic investigation will enhance our understanding of these and related oxides where charge, spin and lattice degrees of freedom are manifested in transport.

ACKNOWLEDGMENTS

This work was supported by NSF Grant No. DMR-9631236.

REFERENCES

1. G. H. Jonker and J. H. Van Santen, *Physica (Amsterdam)* **16,** 337 (1950); J. Volger, *ibid.* **20,** 49 (1954).
2. P. Schiffer *et al., Phys. Rev. Lett.* **75,** 3336 (1995).
3. A. P. Ramirez, *J. Phys. Cond. Matt.* **9,** 8171 (1997).
4. J. B. A. A. Elemans, B. Van Laar, K. R. Van Der Veen, and B. O. Loopstra, *J. Sol. St. Chem.* **3,** 238 (1971).
5. C. Zener, *Phys. Rev.* **82,** 403 (1951); P. W. Anderson and H. Hasegawa, *ibid.* **100,** 675 (1955); K. Kubo and N. Ohata, *J. Phys. Soc. Jpn.* **33,** 21 (1972); N. Furukawa, *ibid.* **63,** 3214 (1994); **64,** 2734 (1995); **64,** 3164 (1995).
6. M. Croft *et al., Phys. Rev. B* **55,** 8726 (1997).
7. H. Röder, J. Zhang, and A. R. Bishop, *Phys. Rev. Lett.* **76,** 1356 (1996); A. J. Millis, B. I. Shraiman, and R. Mueller, *Phys. Rev. Lett.* **77** 175 (1996).
8. J. B. Goodenough, *Phys. Rev.* **100,** 564 (1955).
9. T. Holstein, *Ann. Phys. (N.Y.)* **8,** 343 (1959); N. F. Mott and

E. A. Davis, *Electronic Processes in Non-Crystalline Materials,* (Clarendon Press, Oxford, 1971); D. Emin, *Phys. Rev. Lett.* **35,** 882 (1975); D. Emin, *Physics Today* **35,** No. 6, p. 34 (1982).
10. R. R. Heikes, in *Transition Metal Compounds,* E. R. Schatz, ed. (Gordon and Breach, New York, 1963), p. 1.
11. M. Jaime *et al., Appl. Phys. Lett.* **68,** 11 (1996); *Phys. Rev. B* **54,** 11914 (1996).
12. M. F. Hundley and J. J. Neumeier, *Phys. Rev. B* **55,** 11511 (1997).
13. C. H. Booth *et al., Phys. Rev. Lett.* **80,** 853 (1998); *Phys. Rev. B* **57,** 10440 (1998).
14. M. R. Ibarra *et al., Phys. Rev. B* **56,** 8252 (1997).
15. J. P. Franck *et al., Phys. Rev. B* **58,** 5189 (1998).
16. Some of the author's unpublished data are included for specimens whose thermal conductivities were reported previously in Ref. 17.
17. J. L. Cohn *et al., Phys. Rev. B* **56,** R8495 (1997).
18. M. Jaime *et al., Phys. Rev. Lett.* **78,** 951 (1997).
19. D. C. Worledge, L. Miéville, and T. H. Geballe, *Phys. Rev. B* **57,** 15267 (1998).
20. N. F. Mott, J. *Non-Cryst. Solids* **1,** 1 (1968).
21. T. Holstein, *Phys. Rev.* **124,** 1329 (1961); D. Emin and T. Holstein, *Ann. Phys. (N.Y.)* **53,** 439 (1969)
22. D. Emin, *Philos. Mag.* **35,** 1189 (1977).
23. S. H. Chun, M. B. Salamon, Y. Tomioka, and Y. Tokura, cond-mat/9906198.
24. Y. Tokura *et al., J. Phys. Soc. Jpn.* **63,** 3931 (1994).
25. M. F. Hundley *et al., Appl. Phys. Lett.* **67,** 860 (1995).
26. Y. Tokura *et al., J. Mater. Sci. Eng. B* **31,** 187 (1995).
27. G. J. Snyder *et al., Phys. Rev. B* **53,** 14434 (1996).
28. A. Urishibara *et al., Phys. Rev. B* **51,** 14103 (1995).
29. M. Jaime *et al., Phys. Rev. B* **58,** R5901 (1998).
30. K. Kadowaki and S. B. Woods, *Sol. St. Commun.* **58,** 507 (1986).
31. J. W. Lynn *et al., Phys. Rev. Lett.* **76,** 4046 (1996).
32. I. Mannari, *Prog. Theor. Phys.* **22,** 335 (1959).
33. G. J. Snyder *et al., Appl. Phys. Lett.* **69,** 4254 (1996).
34. P. Wagner *et al., Phys. Rev. B* **55,** R14721 (1997).
35. P. Matl *et al., Phys. Rev. B* **57,** 10248 (1998).
36. G. Jakob *et al., Phys. Rev. B* **57,** 10252 (1998).
37. A. Asamitsu and Y. Tokura, *Phys. Rev. B* **58,** 47 (1998).
38. S. H. Chun, M. B. Salamon, and P. D. Han, *Phys. Rev. B* **59,** 11155 (1999).
39. C. M. Hurd, *The Hall Effect in Metals and Alloys* (Plenum, New York, 1972).
40. W. E. Pickett and D. J. Singh, *Phys. Rev. B* **55,** R8642 (1997).
41. F. E. Maranzana, *Phys. Rev.* **160,** 421 (1967).
42. R. Karplus and J. M. Luttinger, *Phys. Rev.* **95,** 1154 (1954); J. Kondo, *Prog. Theor. Phys.* **27,** 772 (1962).
43. J. P. Jan, *Helv. Phys. Acta* **25,** 677 (1952); J. P. Jan and J. M. Gijsman, *Physica (Amsterdam)* **18,** 339 (1952).
44. T. Okuda *et al., Phys. Rev. Lett.* **81,** 3203 (1998).
45. M. Jaime *et al.,* cond-mat/9808160v2.
46. S. Jin *et al., Science* **264,** 413 (1994).
47. Y. Moritomo, A. Asamitsu, and Y. Tokura, *Phys. Rev. B* **51,** 16491 (1995).
48. J. J. Neumeier *et al., Phys. Rev. B* **52,** R7006 (1995).
49. Y. B. Kim, P. Majumdar, A. J. Millis, and B. I. Schraiman, cond-mat/9803350.
50. Y. Lyanda-Geller, P. M. Goldbart, S. H. Chun, and M. B. Salamon, cond-mat/9904331.
51. J. Ye, Y. B. Kim, A. J. Millis, B. I. Schraiman, P. Majumdar, and Z. Tesanovic, cond-mat/9905007.
52. S. H. Chun, M. B. Salamon, Y. Lyanda-Geller, P. M. Goldbart, and P. D. Han, *Phys. Rev. Lett.* **84,** 757 (2000).
53. C. H. Chen and S.-W. Cheong, *Phys. Rev. Lett.* **76,** 4042 (1996); C. H. Chen, S.-W. Cheong, and H.Y. Hwang, *J. Appl. Phys.* **81,** 4326 (1997); S. Mori, C. H. Chen, and S.-W. Cheong, *Nature* **392,** 473 (1998); *Phys. Rev. Lett.* **81,** 3972 (1998).
54. P. G. Radaelli *et al., Phys. Rev. B* **55,** 3015 (1997).
55. P. G. Radaelli *et al., Phys. Rev. B* **59,** 14440 (1999).
56. Y. Yamada *et al., Phys. Rev. Lett.* **77,** 904 (1996).
57. H. Kuwahara, Y. Moritomo, Y. Tomioka, A. Asamitsu, M. Kasai, R. Kumai, and Y. Tokura, *Phys. Rev. B* **56,** 9386 (1997); Y. Tokura *et al., Phys. Rev. Lett.* **76,** 3184 (1996).
58. H. Y. Hwang, S.-W. Cheong, P. G. Radaelli, M. Marezio, and B. Battlogg, *Phys. Rev. Lett.* **75,** 914 (1995).
59. J. Fontcuberta *et al., Phys. Rev. Lett.* **76,** 1122 (1996).
60. S. Uhlenbruck *et al., Phys. Rev. Lett.* **82,** 185 (1999).
61. L. Pinsard *et al., J. Alloys Compd.* **262, 263,** 152 (1997).
62. P. G. Radaelli *et al., Phys. Rev. B* **56,** 8265 (1997); V. Laukhin *et al., ibid.,* R10009.
63. J.-S. Zhou, W. Archibald, and J. B. Goodenough, *Nature* **381,** 770 (1996).
64. M. Uehara, S. Mori, C. H. Chen, and S.-W. Cheong, *Nature* **399,** 560 (1999).
65. D. E. Cox *et al., Phys. Rev. B* **57,** 3305 (1998).
66. J. Liebe *et al., Appl. Phys. Lett.* **68,** 2343 (1996).
67. D. W. Visser, A. P. Ramirez, and M. A. Subramanian, *Phys. Rev. Lett.* **78,** 3947 (1997).
68. D. G. Cahill, S. K. Watson, and R. O. Pohl, *Phys. Rev. B* **46,** 6131 (1992); D. G. Cahill and R. O. Pohl, *Sol. St. Commun.* **70,** 927 (1989).
69. P. G. Radaelli *et al., Phys. Rev. B* **54,** 8992 (1996); C. H. Booth *et al., ibid.,* R15606 (1996); D. Louca *et al., ibid.* **56,** R8475 (1997).
70. A. Asamitsu *et al., Nature* **373,** 407 (1995); H. Kawano *et al., Phys. Rev. B* **53,** R14709 (1996).
71. M. R. Ibarra *et al., Phys. Rev. Lett.* **75,** 3541 (1995); J. M. De Teresa *et al., Phys. Rev. B* **54,** R12689 (1996); J. J. Neumeier, A. L. Cornelius, and M. F. Hundley, *Mat. Res. Soc. Symp. Proc.* **494,** 293 (1998).
72. A. P. Ramirez *et al., Phys. Rev. Lett.* **74,** 3189 (1995).
73. P. Dai *et al., Phys. Rev. B* **54,** 3694 (1996); *Sol. St. Commun.* **100,** 865 (1996).
74. J. L. Cohn, *Proceedings of the 25th International Thermal Conductivity Conference,* D. T. Morelli and C. Uher, eds. (Technomic, Lancaster, PA, 2000), p. 87.